

# Microstructural development and evolution in liquid-phase sintered Fe–Cu alloys

A. N. NIEMI, T. H. COURTNEY

*Department of Metallurgical Engineering, Michigan Technological University, Houghton, Michigan 49931, USA*

An experimental study relating the scale and contiguity of liquid-phase sintered Fe–Cu alloys to sintering conditions has been conducted over a broad range of solid-phase volume fraction. It is found that the solid-phase contiguity attains a steady-state value at fairly short sintering times and that contiguity increases with increasing particle volume fraction, but is essentially independent of sintering temperature. Both the continuity and scale of microstructure are discussed in terms of concurrent particle coalescence and Ostwald ripening. It is found that values of the probability of particle coalescence after contact required to explain the contiguities observed are in reasonable agreement with theoretical predictions. However, comparison of observed contiguities with those predicted by recent studies is found to be unsatisfactory since the latter do not predict the steady-state contiguities observed. On the other hand, microstructural observations and measurements of coarsening-rate constants as a function of particle volume fraction indicate clearly that particle coalescence contributes significantly to the coarsening process at higher particle volume fractions.

## 1. Introduction

A variety of abrasive, wear-resistant and other parts are produced by liquid-phase sintering processes. The properties of these depend largely on the microstructure developed during sintering [1]. Liquid-phase sintered microstructures are characterized in terms of the volume fraction of solid-phase present during sintering,  $V_p$ , and by the morphology and scale (size) of this solid. Solid-phase morphology is described in terms of contiguity or by the number of solid–solid particle contacts per particle. At a given  $V_p$ , microstructural scale can be quantified by one of several parameters; the number of solid particles per unit volume,  $N_v$ , the average solid particle radius,  $r$ , or the solid–liquid surface area per unit volume,  $S_v$ . In terms of mechanical properties, for example, optimum properties in liquid-phase sintered alloys are generally associated with low solid-phase contiguity and a fine microstructural scale.

This paper is concerned with the basic principles relating to microstructural morphology and scale

in a well-known liquid-phase sintered alloy, Fe–Cu [2–6]. Before describing our experimental work and results and our interpretation of their meaning, it is worthwhile reviewing briefly our approach to understanding the morphology and scale of microstructure in liquid-phase sintered alloys. It is well established that microstructural continuity in liquid-phase sintered alloys derives from the sintering process, rather than from the initial solid-state compaction process. Huppmann and Riegger [7], for example, demonstrated that, in liquid-phase sintered W–Ni alloys, the initial polycrystalline tungsten particles fragmented into small single-crystal particles as a result of nickel penetration along tungsten grain boundaries. Subsequent tungsten contiguity is then developed only by later coalescence of the single-crystal particles. Moreover, in many other liquid-phase sintered alloys the scale of microstructure increases so rapidly with sintering time that it is apparent that solid–solid particle contacts that exist at long sintering times cannot be directly related to the initial cold compaction contiguity [8–10].

There is an inherent dichotomy in the structure of liquid-phase sintered alloys in that wetting is considered necessary for full densification of such materials which contain a high volume-fraction of the solid-phase. That some particles coalesce implies the existence of certain solid–solid orientations for which the wetting relationship does not hold, i.e. that the solid–solid boundaries formed are of low energy. A recent theoretical investigation of coalescence for these cases has been conducted [11]. The results of this work define the fraction of particle contacts made which will lead to a true coalescence event in terms of physico-chemical parameters. This probability,  $p_c$ , is small ( $\leq 10^{-3}$ ) for liquid-phase sintered systems which, on a macroscopic basis, are wetting systems.

## 2. Theoretical background

Courtney [12] has argued that contiguity is determined by competition between two kinetic processes. According to his description, solid particles move about within the liquid as a result of Brownian motion and/or density differences between the solid and the liquid. Hence, solid particles collide with each other, but only a certain fraction,  $p_c$  of these collisions will lead to particle coalescence. If  $\tau_B$  denotes the mean time between particle collisions, then the ratio  $\tau_B/p_c$  is the mean time between particle coalescence. Once coalescence occurs, the particles subsequently fuse into one by the liquid-state analog of the evaporation–condensation mechanism of solid-state sintering. Courtney originally stated that, if the time between coalescence contacts was much greater than the time to fuse the particles subsequent to coalescence,  $\tau_F$ , then an isolated microstructure was developed, and, if the reverse was the case, then a skeletal-type microstructure was formed. Unfortunately, this physically plausible reasoning did not consider that concurrent Ostwald ripening promotes the development of an isolated microstructure. That is, since an isolated structure results if one particle is removed prior to another coalescence event, it is immaterial whether the removal occurs by the fusion of two particles or by Ostwald ripening. Neglecting the time required to remove a particle by Ostwald ripening,  $\tau_{OR}$ , is not too drastic an assumption since  $\tau_{OR}$  is generally greater than  $\tau_F$  because of the small volume of mass required to establish an appreciable neck during particle fusion

as well as the small diffusion distances involved. Nonetheless, in this paper, in terms of establishing a morphological criterion, Courtney's  $\tau_F$  is replaced by  $\tau_{rem}$  where  $\tau_{rem}$  is the effective time taken to remove a particle by concurrent fusion and Ostwald ripening processes.\* Since these processes are parallel, kinetic processes

$$\frac{1}{\tau_{rem}} = \frac{1}{\tau_{OR}} + \frac{1}{\tau_F} \quad (1)$$

or

$$\tau_{rem} = \frac{\tau_{OR}\tau_F}{(\tau_{OR} + \tau_F)}. \quad (2)$$

The above relations serve as a qualitative to semi-quantitative guide to characterizing solid-phase contiguity. Extension of this reasoning, however, allows a quantitative description of the scale of the microstructure. The *total* time taken to remove a particle by coalescence-fusion is  $(\tau_B/p_c + \tau_F)$ . Since this process operates in parallel with Ostwald ripening, the coarsening time,  $\tau_c$ , which is the time to *totally* remove one particle from the system is given by

$$\frac{1}{\tau_c} = \frac{1}{\tau_{OR}} + \frac{1}{\tau_B/p_c + \tau_F}, \quad (3)$$

or

$$\tau_c = \frac{\tau_{OR}(\tau_B/p_c + \tau_F)}{\tau_{OR} + \tau_F + \tau_B/p_c}. \quad (4)$$

If the number of solid particles per unit volume is  $N_v$ , the time rate-of-change of  $N_v$  is given simply as

$$\frac{dN_v}{dt} = -\frac{N_v}{\tau_c}. \quad (5)$$

Equation 3 can be expressed in terms of  $S_v$ , which is measured conveniently, if the particle dispersion is spherical, by utilizing the relations,  $4/3\pi r^3 N_v = V_p$  and  $4\pi r^2 N_v = S_v$ . Taking logarithms of these and differentiating produces

$$\frac{1}{N_v} \frac{dN_v}{dt} + \frac{3}{r} \frac{dr}{dt} = 0 \quad (6)$$

and

$$\frac{1}{N_v} \frac{dN_v}{dt} + \frac{2}{r} \frac{dr}{dt} = \frac{1}{S_v} \frac{dS_v}{dt}. \quad (7)$$

Substitution of  $dr/dt$  from Equation 7 into Equation 6 allows Equation 5 to be written as

$$\frac{1}{S_v} \frac{dS_v}{dt} = -\frac{1}{3\tau_c}. \quad (8)$$

\*“Time taken to remove”, as used in the present context, refers to the time taken to remove a particle under unit particle concentration, e.g., see Equation (5).

The terms in  $\tau_c$  are  $\tau_B$ ,  $\tau_{OR}$  and  $\tau_F$ . The latter are given as [12–14],

$$\frac{\tau_{OR}}{r^3} = \frac{9}{8} \frac{RT}{D_L C_0 \gamma \Omega^2 g(V_p)} = \alpha, \quad (9)$$

and

$$\frac{\tau_F}{r^3} = \frac{KRT}{2D_L C_0 \gamma \Omega^2} = \beta, \quad (10)$$

where  $D_L$  is the diffusion coefficient of solid component (Fe) in the liquid (Cu) (measured in  $m^2 \text{ sec}^{-1}$ ),  $C_0$  is the solubility of solid component (Fe) in liquid (Cu) at the sintering temperature (measured in  $\text{mol m}^{-3}$ ),  $\gamma$  is the liquid (Cu)–solid (Fe) surface energy (measured in  $\text{J m}^{-2}$ ),  $g(V_p)$  is the parameter which takes into account the increased rate of Ostwald ripening with increasing particle volume fraction (dimensionless) [14–16],  $K$  is the parameter which is essentially a normalized time for particle fusion subsequent to a coalescence event (dimensionless) [12],  $R$  is the gas constant and  $T$  is the temperature.  $\tau_B$  is determined by two processes operating in parallel: contacts are formed by both gravity differences and by particle Brownian motion. If the time between the latter is  $\tau_{BR}$  and the time between the former is  $\tau_g$  then

$$\tau_B = \frac{\tau_g \tau_{BR}}{\tau_g + \tau_{BR}}, \quad (11)$$

with [11]

$$\frac{\tau_{BR}}{r^3} = \frac{12\pi\eta}{kT} \left(\frac{\Gamma}{2r}\right)^2, \quad (12)$$

and [11]

$$\frac{\tau_g}{r^3} = \frac{9\eta\Gamma}{2|\Delta-\Delta'|gr^5}, \quad (13)$$

where  $\eta$  is the liquid (Cu) viscosity (measured in  $\text{J sec m}^{-3}$ ),  $\Gamma$  is the mean free distance between particle surfaces (in metres),  $g$  is the acceleration due to gravity (in  $\text{m sec}^{-2}$ ),  $|\Delta-\Delta'|$  is the magnitude of the density difference between the liquid (Cu) and solid (Fe) (in  $\text{kg m}^{-3}$ ) and  $k$  is Boltzman's constant.\* Equations 9–13 can be substituted into Equation 8 which leads to a rather complicated differential equation with a solution of the form

$$t = f_1(S_v) + f_2(S_v). \quad (14)$$

Here,  $f_1(S_v)$  is a series solution in  $S_v$  and  $f_2(S_v)$  is

a cumbersome analytical function of  $S_v$ . Inspection of Equation 14 in this form gives little insight into the kinetic form of the coarsening process. The latter can be deduced, however, by considering two limiting cases. In one,  $\tau_B/p_c \gg \tau_{OR}\tau_F$  and the other corresponds to the opposite conditions. For the former, coarsening is controlled solely by Ostwald ripening and hence  $\tau_c = \tau_{OR}$  and

$$\frac{1}{S_v} \frac{dS_v}{dt} = -\frac{1}{3\alpha r^3}. \quad (15)$$

Using the relationships between  $r$ ,  $S_v$  and  $N_v$  this equation integrates to

$$\frac{1}{S_v^3} - \frac{1}{S_{v0}^3} = \frac{t}{27V_p^3\alpha}, \quad (16)$$

where  $S_{v0}$  is the original particle–matrix surface area per unit volume. Equation 16 is nothing more than an alternative expression of the more common equation relating particle size to coarsening time as given by the Lifshitz–Sylozov–Wagner analysis and its subsequent modifications [15–19]. The other extreme case corresponds mathematically to  $\tau_B/p_c \rightarrow 0$  and  $\tau_c = \tau_{OR}\tau_F/\tau_{OR} + \tau_F$  for which

$$\frac{1}{S_v} \frac{dS_v}{dt} = -\frac{1}{3} \frac{(\alpha + \beta)}{\alpha\beta r^3}, \quad (17)$$

which integrates to

$$\frac{1}{S_v^3} - \frac{1}{S_{v0}^3} = \frac{t}{27V_p^3} \frac{(\alpha + \beta)}{\alpha\beta}. \quad (18)$$

Both Equations 16 and 18 predict equivalent kinetics; however, the effective time constant ( $\alpha$ , or  $\alpha\beta/\alpha + \beta$ ), which is designated as  $\tau_c/r^3$ , will vary between

$$\frac{\tau_{OR}}{r^3} \geq \frac{\tau_c}{r^3} \geq \frac{\tau_{OR}\tau_F}{\tau_{OR} + \tau_F}. \quad (19)$$

While similar kinetics are not predicted for the general case (although one intuitively suspects that, within experimental accuracy, they may be the same), the effective time constant should vary between the limits shown above. Hence a transition in the dominant coarsening mechanism with, say,  $V_p$  which affects  $\tau_{OR}$  and  $\tau_F$  in different ways,

\*Equations 12 and 13 are appropriate for isolated particles. For skeletal structures, the “particles” that move about are generally “clumps” of connected portions of spheres. In this case, the  $r$ -term, which represents a drag force, should be replaced by a suitable value of the particle volume surface area ratio. In the analysis that follows, Equations 12 and 13 are used, as written, in Equation 11. When applied to skeletal structures, this will result in an error in the values of  $p_c$  that are deduced. However, the mere fact that a skeletal structure exists implies that  $\tau_B < \tau_{rem}$  and hence, utilization of Equations 12 and 13 will not substantially change any of the conclusions arrived at later.

should be accompanied by noticeable changes in  $\tau_c/r^3$  and it is this premise that will be used as a basis for subsequent discussion.

### 3. Experimental procedure

Powder compacts were fabricated from plasma-sprayed iron (99.9% purity) and copper (99.0% purity) powders. Elemental powders were mixed together to yield 40, 50, 60 and 70 vol% Fe alloys. After blending, powders were cold compacted at a pressure of  $260 \text{ MN m}^{-2}$  into 0.79 cm diameter cylindrical slugs. The samples, approximately 0.65 cm in height, had a green density of about 70%, theoretical.

After an oxide reduction in hydrogen at a temperature of 1173 K, the samples were liquid-phase sintered, also under a flowing hydrogen atmosphere, at temperatures of 1423, 1523 and 1573 K for times up to 192 h. All alloy compositions were sintered at 1423 K, but only the 70 vol% Fe samples were sintered at the higher temperatures. As determined by periodic checking with a thermocouple, sintering temperatures remained constant within  $\pm 2 \text{ K}$  over the sintering runs. After sintering, the samples were withdrawn rapidly into the cool end of the furnace tube.

Quantitative metallography was performed on suitably prepared metallographic samples. The interfacial surface area per unit volume,  $S_v$ , was determined using the line intercept method [20] and volume fractions were also occasionally determined as a check on composition. Solid-phase contiguity was initially determined using the method described by Gurland [21]. However, due to the low contiguities involved, it was found that the number of inter-particle contacts per particle on a two-dimensional plane of polish,  $C_p$ , was a more sensitive measure of contiguity.  $C_p$  values were determined by counting the number of inter-particle contacts made by each particle intersected by a random line. It was also necessary to define at what stage of particle fusion "two" particles should be considered as "one". In this regard, it was postulated that if the neck diameter was at least two-thirds of the diameter of the smaller of the contacting particles, the particles were considered as having fused into one. Measurement of at least 1000 particle-matrix line intercepts and 100 inter-particle contacts were necessary to obtain accurate values for  $S_v$  and  $C_p$ .

### 4. Experimental results

Micrographs representative of the alloys studied in this investigation are shown in Fig. 1. Fig. 1 shows that the number of inter-particle contacts and the average particle size increase with increasing solid volume-fraction at constant sintering time and temperature. As expected, the average particle size increases with increasing sintering temperature. Fig. 2 also shows some interesting features of the structures observed. Fig. 2a clearly indicates that extensive coalescence occurs in the alloys studied, a feature also demonstrated in Fig. 2b wherein pockets of liquid copper are shown between coalesced solid Fe-particles. Although several of the pockets appear to be completely isolated in three, as well as two, dimensions they need not be so in order to demonstrate evidence of coalescence.

Contiguity data in the form of  $C_p$  values are presented in Table I wherein it can be seen that steady-state values of  $C_p$  are approximately attained for sintering times in excess of about 16 hours. The exception to this is the 70 vol% Fe alloy sintered at 1573 K for which some evaporation of liquid copper occurred. Indeed, it was found that, for this sintering treatment, samples had to originally contain slightly less than 70 vol% Fe in order to maintain an average value of 70 vol% Fe after sintering. The data of Table I are summarized in the form of a "microstructure map" shown in Fig. 3, wherein the axes are the solid-particle volume-fraction and the sintering variable, temperature, and the "data points" are the steady-state values of  $C_p$ . The map is divided, somewhat arbitrarily, into regions representing "skeletal" and "non-skeletal" microstructures. As indicated by large values of  $C_p$ , high solid-phase volume-fraction leads to skeletal microstructures and vice-versa. Within the accuracy of the experimental results, sintering temperature has little effect on the steady-state morphology. In Fig. 3, the division between skeletal and non-skeletal microstructures corresponds to approximately 0.75 two-dimensional contacts per particle. The criterion for separating skeletal and non-skeletal microstructures was also based on experimental observations of the compact shape during sintering. Low solid-phase volume-fraction composites slumped rapidly during sintering and this has been attributed to the non-skeletal geometry of the solid particles. Higher volume-fraction solid compacts also slumped during sintering, but at a rate considerably reduced in comparison to low solid-phase volume-fraction

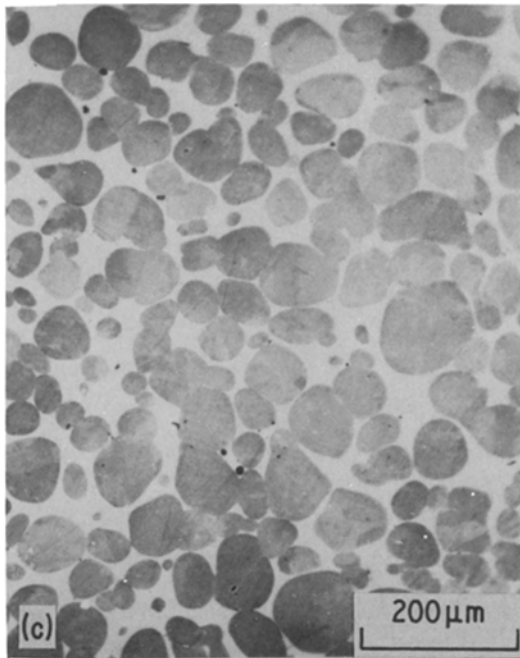
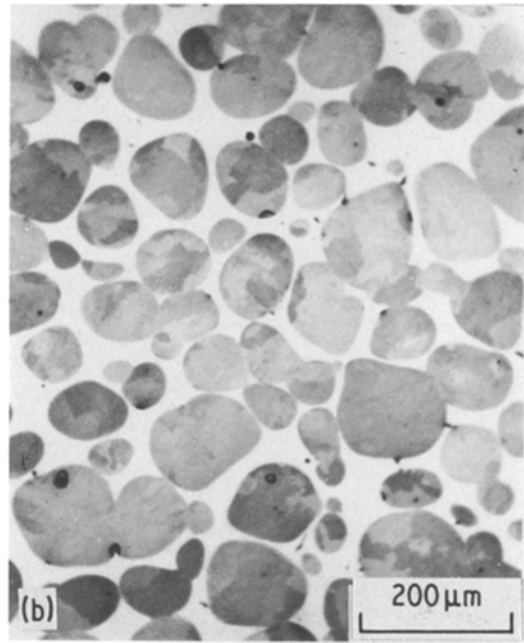
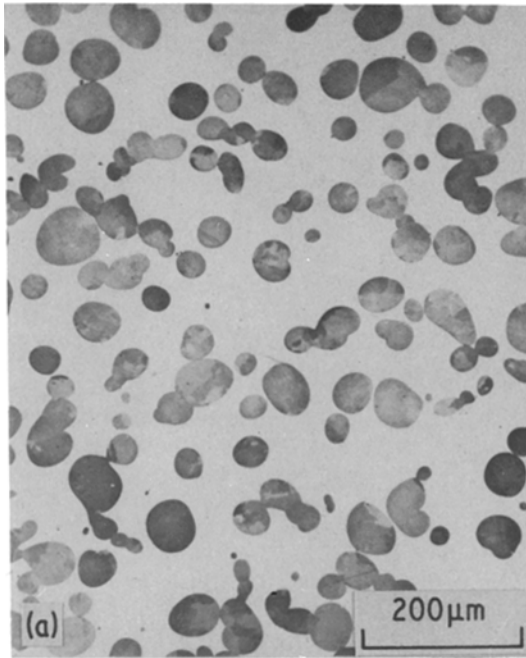


*Figure 1* Effect of sintering temperature and solid-phase volume-fraction on microstructures developed in Fe–Cu liquid-phase sintered alloys. Sintering time = 24 h. (a) 40 vol% Fe, sintering temperature = 1423 K; (b) 70 vol% Fe, sintering temperature = 1523 K; (c) 70 vol% Fe, sintering temperature = 1423 K. Increasing the sintering temperature (compare (c) and (b)) and the solid-phase volume-fraction (compare (b) and (a)) produce coarser microstructures.

compacts. Although slumping could intuitively be expected not to occur in a skeletal structure it must be realized that the microstructure is a dynamic one wherein contacts are continually formed and particles continually dissolved during sintering. This dynamic process allows slumping to proceed at a perceptible rate even though the instantaneous structure is classified as skeletal.

Table II summarizes the effects of sintering time, temperature, and solid-phase volume-fraction on  $S_v$ . As expected,  $S_v$  decreases with isothermal sintering time and, at constant  $V_p$  and sintering time, with increasing sintering temperature. The adequacy of the time exponent in Equations 16 and 18, with respect to the data reported here, can be checked by plotting  $\log S_v$  against  $\log t$  (where  $t$  is the sintering time) in the region where  $1/S_v^3 \geq 1/S_{v0}^3$ . This is done in Fig. 4 where the expected slope of  $-1/3$  is in good agreement with the experimentally derived slopes. Values of  $\tau_c/r^3$  were determined by plotting  $1/S_v^3$  against sintering time; several examples of these plots are shown in Fig. 5 which indicates that subsequent to the development of a steady-state microstructure (and indeed, before this development, for many samples), the relationship between  $1/S_v^3$  and sintering time is linear. Values of  $\tau_c/r^3$  as obtained from the slopes of these lines are represented in Table II.

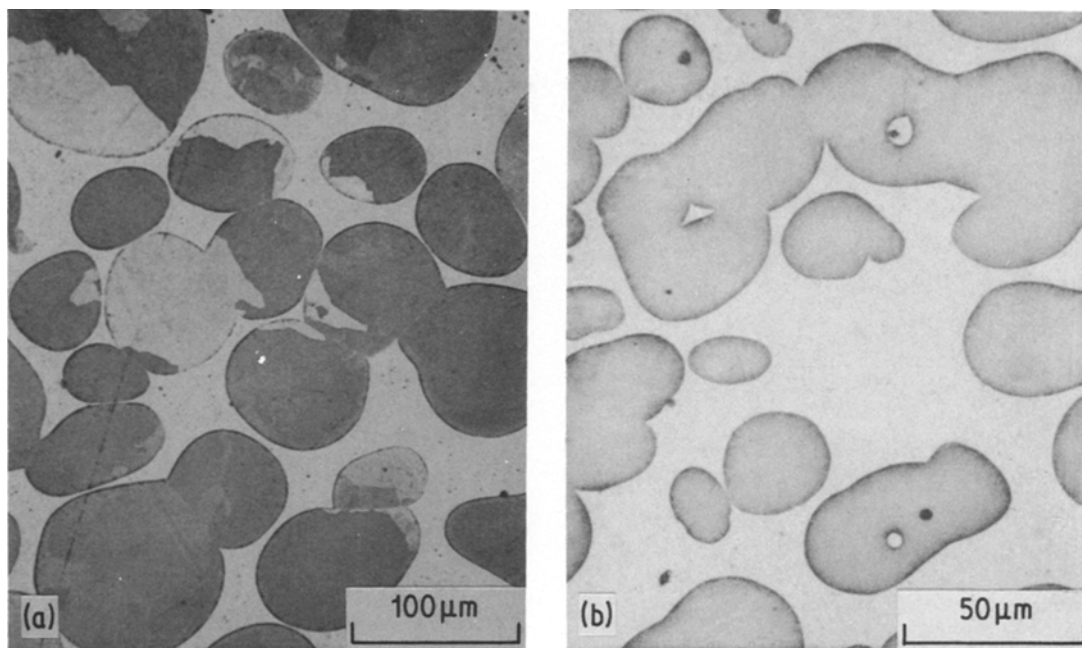


Figure 2 (a) 70 vol% Fe–Cu alloy sintered for 48 h at 1423 K. Considerable evidence of coalescence is shown; note that subsequent to the coalescence event, grain-boundary migration away from the original neck has occurred. (b) 60 vol% Fe–Cu alloy sintered for 2 h at 1423 K; coalescence is evidenced by the entrapment of liquid copper between Fe-grains. ((a) and (b) were etched differently so that grain boundaries are not evident in (b).)

## 5. Discussion

The microstructure developed, as a function of the solid-phase volume-fraction, can be discussed using an approach similar to that presented in Sections 1 and 2. According to the reasoning therein, a skeletal microstructure is formed if  $\tau_B/p_c \ll \tau_{rem}$  and, if the reverse is true, a non-skeletal microstructure is formed. In Fig. 6, these parameters, as calculated from Equations 9–11 utilizing the ancillary data shown in Table III, are plotted for two different particle sizes ( $r = 25 \mu\text{m}$ , Fig. 6a;  $r = 60 \mu\text{m}$ , Fig. 6b) which correspond approximately to experimental particle sizes for sintering

times at 1423 K of 16 and 192 h, respectively (i.e. the range of “steady-state” microstructures). From the ancillary data employed (the uncertainty in which can, as will presently be shown, lead to an order of magnitude error in calculated values of  $\tau$ )  $\tau_B \ll \tau_{BR}$ , and hence  $\tau_B/\tau_{rem}$ , will be a function of particle size (compare Fig. 6a and b). Also, in calculating  $\tau_{rem}$ ,  $g(V_p)$ , as deduced by Brailsford and Wynnblatt [14], has been utilized (previously derived formulations do not appear as accurate as these most recent ones) and the values of  $\Gamma/2r$  used in the calculations were obtained from the relationships presented by Fullman [22]. As can

TABLE I Two-dimensional contacts per particle,  $C_p$ , as a function of sintering time, temperature, and solid volume-fraction,  $V_p$

$V_p$	$T$ (K)	Sintering time (h)							$C_{pss}^*$
		1	8	16	24	48	96	192	
0.4	1423	0.64	–	–	0.64	0.82	0.53	0.85	$0.71 \pm 0.15$
0.5	1423	0.71	1.00	–	0.82	0.83	0.62	–	$0.76 \pm 0.12$
0.6	1423	1.55	–	–	0.97	0.91	0.85	1.00	$0.93 \pm 0.07$
0.7	1423	1.55	1.55	1.06	1.20	–	1.10	1.20	$1.14 \pm 0.07$
0.7	1523	1.30	1.30	–	1.50	1.40	–	–	$1.45 \pm 0.07$
0.7	1573	–	0.95	–	1.10	1.48	–	–	$1.29 \pm 0.27$

\* $C_{pss}$  is the steady state contiguity.

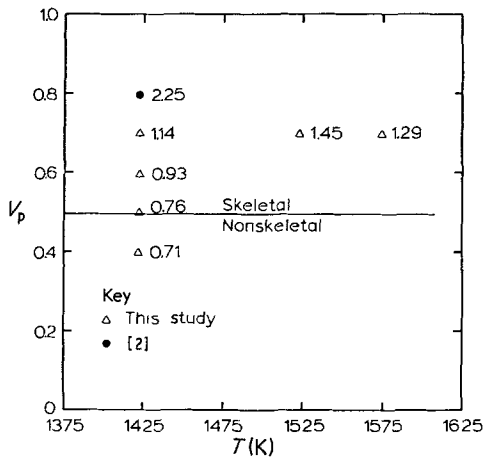


Figure 3 A microstructure map indicating the effect of solid-phase volume-fraction,  $V_p$ , on steady-state solid contiguity. Contiguity is measured by the number of two-dimensional contacts per particle,  $C_p$ , and the transition from a skeletal to a non-skeletal microstructure occurs at  $C_p \sim 0.75$ , i.e. at  $V_p \sim 0.5$ .

be seen in Fig. 6, two curves of  $\tau_{rem}$ , as a function of  $V_p$ , are shown; one corresponds to a constant value of  $K$  ( $K = 0.161$ ) in  $\tau_F$  and the other corresponds to  $K$  varying with  $V_p$  ( $K = K(V_p)$ ). This latter curve is related to the work of Courtney [14] wherein an attempt was made to take account of the fact that  $\tau_F$  should increase with increasing

$V_p$  because of a decrease in the area available for diffusion attendant with increases in  $V_p$ . Courtney assumed a cubic close-packed particle array and this unjustified approximation led him to underestimate the diffusion area and, consequently, unrealistically over-estimate the effect of  $V_p$  on  $\tau_F$ . The curves shown in Fig. 6a and b for  $K = K(V_p)$  are calculated according to Courtney's original scheme, but the cubic close-packed array has been replaced by a random array of dispersed particles. The curve for  $K = 0.161$  corresponds to  $\tau_F$  for  $V_p = 0$  for which no arbitrary geometrical assumptions were made and hence we believe that the actual value of  $\tau_{rem}$  should lie somewhere in the region between the curves drawn in Fig. 6. According to Fig. 6, the morphology of our alloys can be justified if  $p_c \sim 10^{-4}$  for  $r = 25 \mu m$  and  $p_c \sim 3 \times 10^{-6}$  for  $r = 60 \mu m$ , since these correspond to skeletal microstructures forming at  $V_p \sim 0.5$ . It should be noted that these conditions are *not* consistent with our experimental results in that, if a constant value of  $p_c$  were to pertain throughout, either the contiguity should increase with increasing sintering time because of the increased particle size or, equivalently, skeletal microstructures should develop at lesser values of  $V_p$  at larger sintering times. That this is not observed may be due to an underestimate in  $\tau_g$  (as a result of an overestimate

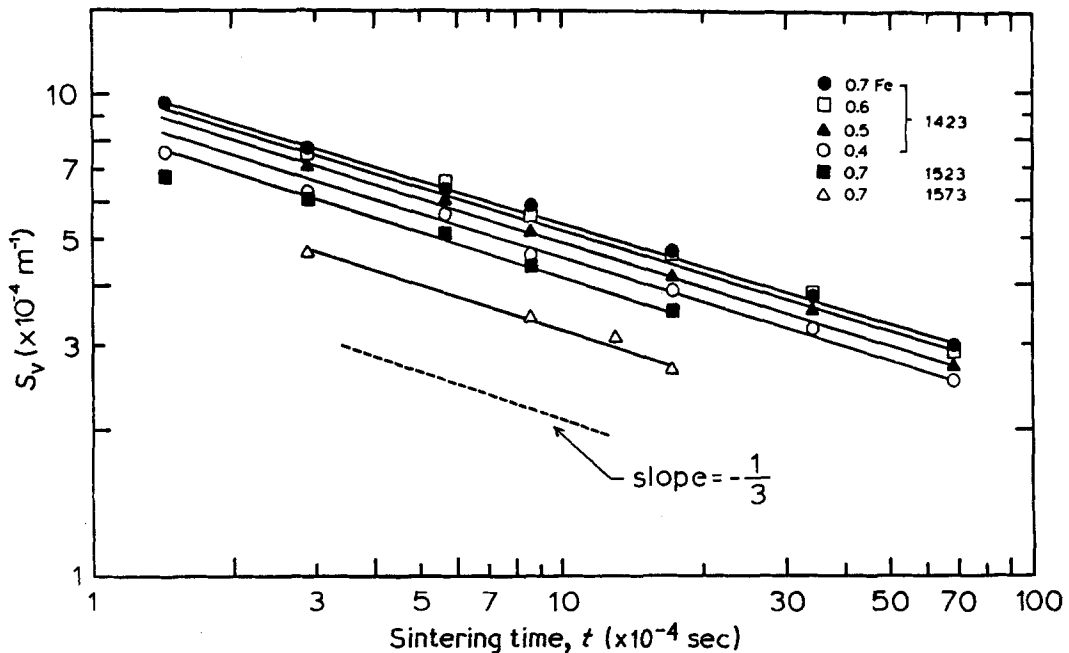


Figure 4 Plot of particle surface-area per unit volume,  $S_v$ , against sintering time,  $t$ . A slope of  $-1/3$  on the logarithmic co-ordinates employed indicates that the kinetics predicted by Equations 16 and 18 are observed.

TABLE II Experimentally determined surface-to-volume ratio,  $S_v$ , and rate constant,  $\tau_c$ , as a function of sintering time, temperature, and solid volume-fraction,  $V_p$ .

$V_p$	$T$ (K)	$S_v (\times 10^{-4} \text{ m}^{-1})^*$										$\tau_c / r^3$ ( $\times 10^{-18} \text{ sec m}^{-3}$ ) <sup>†</sup>
		Time = 1 h	Time = 2 h	Time = 4 h	Time = 8 h	Time = 16 h	Time = 24 h	Time = 48 h	Time = 96 h	Time = 192 h		
0.4	1423	11.4	10.1	7.6	6.3	5.6	4.66	3.89	3.22	2.55	6.76	
0.5	1423	13.5	9.1	10.0	7.2	6.1	5.2	4.17	3.53	2.68	4.07	
0.6	1423	13.5	10.1	10.0	7.7	6.5	5.7	4.64	3.82	2.94	3.10	
0.7	1423	12.7	12.1	9.6	7.8	6.4	5.9	4.66	3.80	3.02	2.08	
0.7	1523	10.3	9.1	6.8	6.1	5.1	4.40	3.52	—	—	0.72	
0.7	1573	—	—	—	4.71	3.43	2.68	(3.10 for $t = 36 \text{ h}$ )	—	—	0.36	

\*Estimated error in  $S_v$ ,  $\Delta S_v / S_v \sim 0.02$ .

†Estimated error in  $\tau_c$ ,  $\Delta \tau_c / \tau_c \sim 0.06$ .

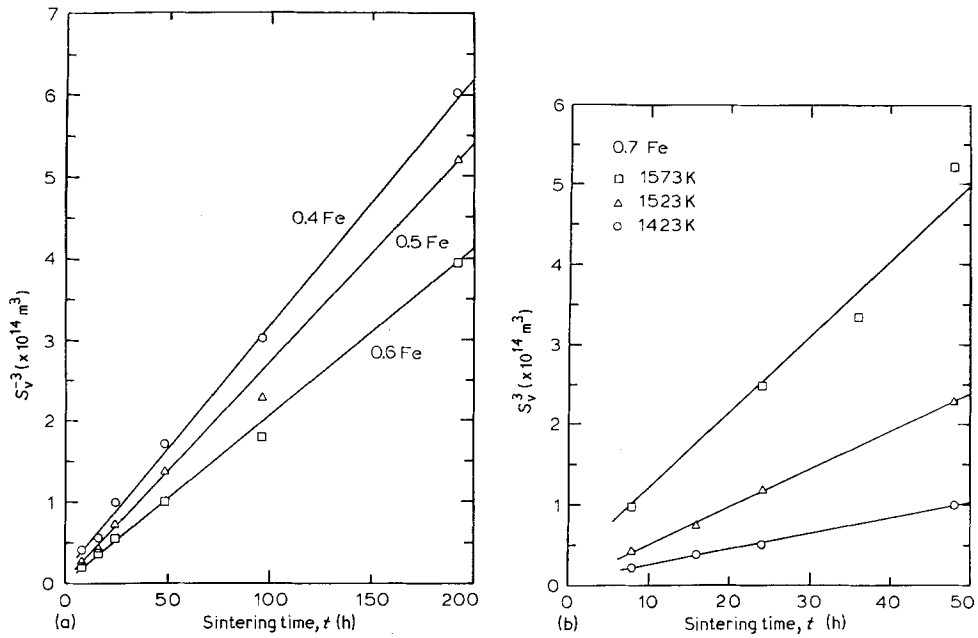


Figure 5 Example graphs of  $1/S_v^3$  against sintering time,  $t$ . (a) Sintering temperature = 1423 K; illustrates the effect of  $V_p$  on  $\tau_c/r^3$ . (b) 70 vol% Fe; illustrates the effect of sintering temperature on  $\tau_c/r^3$ .

in  $|\Delta - \Delta'|$ ). On the other hand, for volume-fractions in which a skeletal microstructure is established at an early stage, an observed large change in contiguity would not be expected since a particle must be "worked free" prior to producing a new

contact via gravity and the time required for this ( $\geq \tau_{rem}$ ) is much greater than  $\tau_B$ . It is wished to point out that, based on recent theoretical calculations of  $p_c$  in wetting systems [11], the small values of  $p_c$  required to justify the transition from

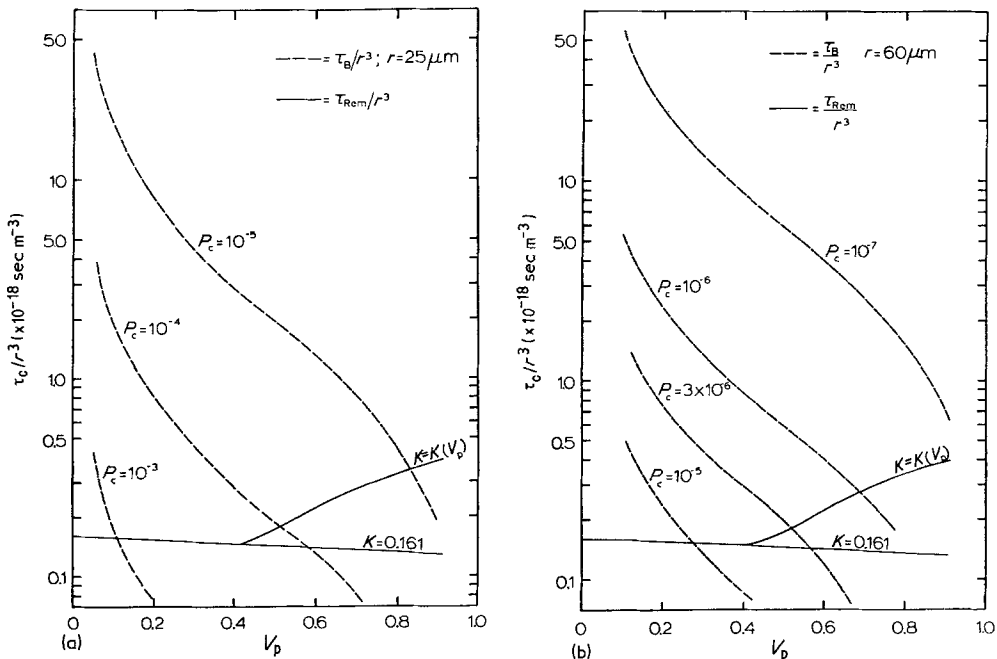


Figure 6 Calculated values of  $\tau_B/p_c r^3$  and  $\tau_{rem}/r^3$  plotted against  $V_p$ . Ancillary data from Table III were used in the calculations. For a transition from skeletal to a non-skeletal structure at  $V_p \sim 0.5$ ,  $p_c \sim 10^{-4}$  for  $r = 25 \mu\text{m}$  and  $p_c \sim 3 \times 10^{-6}$  for  $r = 60 \mu\text{m}$ .

TABLE III Ancillary data used in calculating rate constants at a temperature of 1423 K

Parameter	Value	Reference source for data
$D_L$	$4.53 \times 10^{-9} \text{ m}^2 \text{ sec}^{-1}$	[23]
$C_o$	$5.94 \times 10^3 \text{ mol m}^{-3}$	
$\gamma_{SL}$	$0.375 \text{ J m}^{-2}$	[2]
$\Omega$	$7.36 \times 10^{-6} \text{ m}^3 \text{ mol}^{-1}$	[24]
$\eta$	$3.55 \times 10^{-3} \text{ J sec m}^{-3}$	[25]
$ \Delta - \Delta' $	$290 \text{ kg m}^{-3}$	[26]

a skeletal to a non-skeletal microstructure are reasonable.

The above arguments are useful only insofar as rationalizing order-of-magnitude values of  $p_c$  necessary for a non-skeletal – skeletal transition with increasing  $V_p$ . As noted previously, however, the relative contributions of coalescence and Ostwald ripening to microstructural coarsening can be ascertained approximately by considering the dependence of  $\tau_c/r^3$  on  $V_p$ . The ancillary data from Table III predict values of  $\tau_{OR}/r^3$  which are an order of magnitude greater than the observed values of  $\tau_c/r^3$ . Uncertainties of the order of 30% in the parameters utilized in this calculation account for such an order-of-magnitude discrepancy and therefore an attempt will be made to separate the contributions coarsening of coalescence and Ostwald ripening by consideration of the dependence of  $\tau_c/r^3$  on  $V_p$ . The experimental data are shown in Fig. 7. The dotted lines shown in Fig. 7 correspond to the  $V_p$  dependence of  $\tau_{OR}$  and  $\tau_{OR}\tau_F/\tau_{OR} + \tau_F$ . In constructing the magnitudes (but not the shapes) of the experimental curve, one experimental data point, at  $V_p = 0.4$  has been arbitrarily fitted to the curve corresponding to  $\tau_{OR}/r^3$ . It can be seen that the  $V_p$  dependence of  $\tau_c/r^3$  is considerably different from that predicted theoretically for Ostwald ripening\* alone and, indeed, the force-fit of one data point leads to an excellent correlation with experimental results in that a transition from coarsening dominated by Ostwald ripening to that dominated by coalescence occurs at  $V_p \sim 0.50-0.60$ . Although it is felt that these arguments give strong evidence that coalescence affects coarsening in the system, it is realized that the force-fitting of even one data point is not appealing. As additional evidence that coalescence does affect coarsening and the microstructural development of this system, Fig. 8 shows the

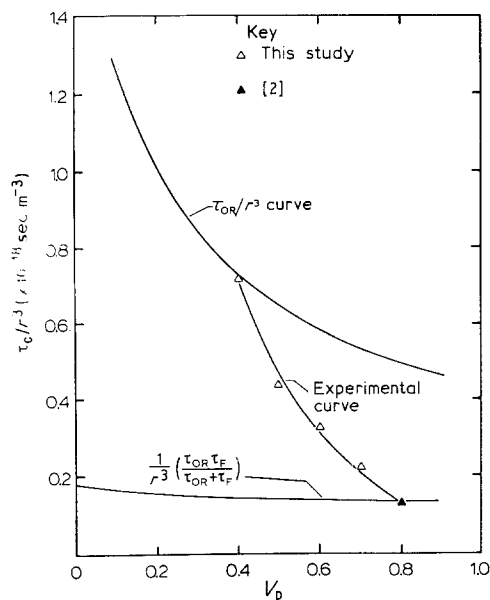


Figure 7 Experimental and theoretical curves of  $\tau_c/r^3$  against  $V_p$ . The theoretical curves correspond to the limiting cases discussed in the text. The experimental data, after force-fitting one data point at  $V_p = 0.40$  to the theoretical curve for  $\tau_{OR}/r^3$ , is consistent with the microstructures observed and the shape of the experimental curve can be explained only if coalescence becomes important during coarsening for values of  $V_p \geq 0.5$ .

experimentally measured rate constant as a function of  $C_p$ . Although the relationship shown is not of fundamental significance it shows clearly that there must exist a transition in the coarsening mechanism in the vicinity of  $C_p \sim 0.5$ . This is so

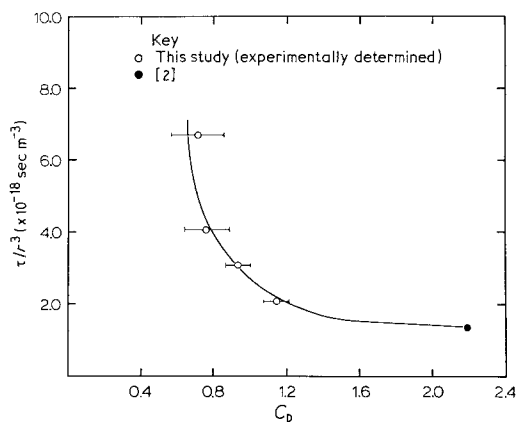


Figure 8 Empirical relationship between  $\tau_c/r^3$  and  $C_p$  for liquid-phase sintered Fe-Cu alloys. When  $C_p \rightarrow 0$ ,  $\tau_c/r^3 \rightarrow \tau_{OR}/r^3$ ; hence some transition in the coarsening mechanism must occur for  $C_p \leq 0.5$ .

\*Utilizing alternative expressions for  $g(V_p)$  would not alter this conclusion.

because, due to Ostwald ripening, the coarsening rate cannot go to zero (i.e. the ratio  $\tau_c/r^3$  cannot go to infinity) as  $C_p$  goes to zero. The transition at  $C_p \sim 0.5$  corresponds to  $V_p \sim 0.4$  which is, of course, near the transition point previously observed.

Finally, microstructural morphology is, without doubt, the most convincing optical evidence for the contribution of coalescence to coarsening (compare with Figs. 1 and 2). Certainly, based on this evidence, coalescence contributes to the evolution and development of microstructure in liquid-phase sintered Fe—Cu alloys.

### Acknowledgments

The authors appreciate the efforts of Mr. Ayo Momo who aided considerably in the quantitative metallographic studies and are grateful to the Army Research Office for financial support of this programme.

### References

1. M. J. HUMENIK and N. M. PARIKH, *J. Amer. Ceram. Soc.* **39** (1956) 60.
2. R. WATANABE and Y. MASUDA, *Trans. Jap. Inst. Met.* **14** (1973) 320.
3. P. RAMAKRISHNAN and R. LAKSHMINARISIMHAN, *Int. J. Powder Met.* **3** (1967) 63.
4. W. D. KINGERY, *J. App. Phys.* **30** (1959) 301.
5. W. D. KINGERY and M. D. NARASINHAN, *ibid.* **30** (1959) 307.
6. F. V. LENEL, *Trans. TMS-AIME* **175** (1945) 878.
7. W. J. HUPPMANN and H. RIEGGER, *Int. J. Powder Met. and Powder Tech.* **13** (1977) 243.
8. THAE-KHAPP KANG and D. N. YOON, *Met. Trans. A* **9A** (1978) 433.
9. R. WARREN, *J. Mater. Sci.* **7** (1972) 1434.
10. N. C. KOTHARI, *J. Less Common Met.* **13** (1967) 457.
11. T. H. COURTNEY and J. K. LEE, *Met. Trans.* **11A** (1980) 943.
12. T. H. COURTNEY, *Met. Trans. A* **8A** (1977) 679.
13. *Idem, ibid.* **8A** (1977) 685.
14. *Idem, ibid.* **8A** (1977) 671.
15. A. D. BRAILSFORD and P. WYNBLATT, *Acta Met.* **27** (1979) 489.
16. A. J. ARDELL, *ibid.* **20** (1972) 61.
17. R. ASIMOW, *ibid.* **11** (1963) 72.
18. C. WAGNER, *Z. Elektrochem* **65** (1961) 581.
19. I. M. LIFSHITZ and V. V. SYLOZOV, *J. Phys. Chem. Sol.* **19** (1961) 35.
20. C. S. SMITH and L. GUTTMAN, *Trans. TMS-AIME* **197** (1953) 81.
21. J. GURLAND, *ibid.* **236** (1966) 642.
22. R. L. FULLMAN, *ibid.* **197** (1953) 447.
23. T. EJIMA and M. KAMEDA, *J. Japan Inst. Met.* **33** (1969) 96.
24. B. D. CULLITY, "Elements of X-ray Diffraction" (Addison-Wesley, Reading, Massachusetts, 1967) p. 483.
25. "The Making, Shaping and Treating of Steel" 9th edition (U.S. Steel Corporation, Pittsburgh, 1971) p. 337.
26. "CRC Handbook of Chemistry and Physics" 51st edition (1970–71) B-235.

Received 27 March and accepted 30 June 1980.